# Application of a new concept for multi-scale interfacial structures to the dam-break case with an obstacle

Hänsch, S.; Lucas, D.; Höhne, T.; Krepper, E.;

Originally published:

March 2014

**Nuclear Engineering and Design 279(2014), 171-181**

DOI: https://doi.org/10.1016/j.nucengdes.2014.02.006

Perma-Link to Publication Repository of HZDR:

https://www.hzdr.de/publications/Publ-19132

# Application of a new concept for multi-scale interfacial structures to the dam-break case with an obstacle

Susann Hänsch*, Dirk Lucas, Thomas Höhne, Eckhard Krepper

Helmholtz-Zentrum Dresden-Rossendorf e.V.,

Institute of Fluid Dynamics, POB 51 01 19, 01314 Dresden, Germany

*Corresponding author. Tel. +49 351 260 3157, E-mail: s.haensch@hzdr.de

ABSTRACT

New results of a generalized concept developed for the simulation of two-phase flows with multi-scale interfacial structures are presented in this paper. By extending the inhomogeneus Multiple Size Group-model, the concept enables transitions between dispersed and continuous gas morphologies, including the appearance and evanescence of one of these particular gas phases. Adequate interfacial transfer formulations, which are consistent with such an approach, are introduced for interfacial area density and drag. A new drag-formulation considers shear stresses occurring within the free surface area.

The application of the concept to a collapsing water column demonstrates the breakup of continuous gas into a polydispersed phase consisting of different bubble sizes. Both resolved free surface structures as well as the entrainment of bubbles and their coalescence and breakup underneath the surface can be described. The simulations have been performed with the CFD-code CFX 14.0 and will be compared with experimental images.

The paper will further investigate the possible improvement of such free surface simulations by including sub-grid information about small waves and instabilities at the free surface. A comparison of the results will be used for a discussion of possible new mass transfer models between filtered free surface areas and dispersed bubble size groups as part of the future work.

Keywords: multi-scale, flow regime transitions, air entrainment, dam-break, MUSIG, AIAD

# 1 INTRODUCTION

Nuclear reactor thermal hydraulics generally involves complex multiphase flows. Concerning nuclear safety issues, reliable predictions of accident scenarios include various steam-water flows and especially flow regime transitions. Based on the structure of gas-liquid interfaces different gaseous morphologies occur, like continuous or dispersed gas phases.

According to the scale of interfacial structures relative to the size of the computational grid, resolving and averaging methods are established for the numerical simulation of multiphase flows. The Eulerian two-fluid model describes small-scale bubbly flows. When investigating such flow patterns, characterized by an interfacial scale smaller than grid size, an averaged treatment is used and for each phase a corresponding set of equations is solved. The inhomogeneous Multiple Size Group (MUSIG) – model (e.g. Krepper et al., 2008) extends the two-fluid model to a multi-field two-fluid model. It has been successfully applied to very complex dispersed flows, consisting of bubbles with different sizes and associated velocity fields. For flow situations with large-scale interfacial structures interface capturing methods are applied, like Volume-Of-Fluid (VOF) - or Level-Set-methods. For those cases the computational grid should be fine enough for a localization of the gas-liquid interface allowing a detailed resolution of surface phenomena.

However, many practical applications cover a wide range of interfacial scales and frequently transitions between different morphologies occur. Therefore, all gas structures with interfacial scales smaller than grid size require an averaged treatment for bubbly flows, while gas structures larger than grid size should be determined by an interface capturing method. An open question remains the gap in the scales for intermediate ranges of interfacial structures pointed out by Tomiyama et al. (2006). First approaches in literature are available and try to couple interfacial scale averaging and -resolving

techniques. Some of them explicitly couple the two-fluid model with a VOF-method (e. g. Černe et al., 2001; Yan and Che, 2010) or a Level-Set approach (Tomiyama and Shimada, 2001). Other authors use an imitation of interface capturing methods within the two-fluid model (e. g. Štrubelj et al., 2009; Coste, 2013). As a result of the averaging procedure the captured interface then is filtered and sub-grid information about it has disappeared (Bestion, 2012). Mass transfers between dispersed phase-averaged and continuous resolved gaseous morphologies have not been considered sufficiently so far and need to be investigated carefully. Of particular interest are the cases, which include the evanescence or appearance of one of those phases. Such a multi-scale approach is necessary to predict changes of the flow regime, being important for many accidental scenarios of nuclear reactors and many other industrial applications.

This paper presents a recently developed concept for generalized two-phase flows (GENTOP), resuming the idea of interface capturing within an Eulerian multi-field framework (Hänsch et al., 2012). Using the scopes of the inhomogeneous MUSIG-model changes in gaseous morphology are considered and investigated. The drag at detected free surfaces is modelled using a formulation given by Höhne and Vallée (2010). The concept has been successfully applied to different demonstration cases, which involve various flow regime transition (Hänsch et al., 2012). The air entrainment process, occurring with impinging jets, represents the transition from a resolved to a polydispersed gas phase and was reproduced using the new concept. The inverse transfer from dispersed into continuous structures was demonstrated with the appearance of a chain of large bubbles in a bubble column. This paper is intended to improve the concept by introducing small wave turbulence within the free surface region of the continuous gas. The sub-grid information about small waves and instabilities at the surface, which is lost using an averaged framework, is retrieved via source terms of turbulent kinetic energy following a proposal of Brocchini and Peregrine (2001). Comparative simulations are

performed using a new demonstration case, which follows the dam-break experiment performed by Koshizuka et al. (1995). This test case of a liquid column collapse hitting an obstacle demonstrates the transition from a continuous gas into a polydispersed phase. Later on the inverse mass transfer occurs, when the flow field separates again leaving only continuous gas behind.

# 2 DESCRIPTION OF THE MULTI-FIELD CONCEPT

## 2.1 MAIN CONCEPT

Currently, the GENTOP-concept is illustrated using a three-field two-fluid simulation. The flow field is described using a continuous liquid phase $l$, a polydispersed gas phase $dg$ and a potentially continuous gas phase $cg$. Formally, the concept extends the inhomogeneous MUSIG-model, as it is demonstrated in Fig. 1. The gas phases are divided into a number of $N$ velocity fields. The overall bubble size distribution is further split into sub-size fractions $M_j$, that are allocated to the different velocity fields. Each size fraction $i$ ($i = 1,...,M_j$) represents bubbles of a certain diameter $d_i$. An occupation number $f_i = \alpha_i / \alpha_j$ shows the contribution of each size group to the total volume fraction of a gas phase. For the largest gas structures a potentially continuous gas phase $cg$ is introduced, being the last velocity group and described by an own set of mass and momentum equations. It consists of a virtual size group and represents all gas structures that exceed a certain maximum bubble diameter $d_{dg,\max}$ of the polydispersed gas $dg$. Consequently, three different sets of mass- and momentum equations are solved. Governing equations are the continuity and momentum equations for a gaseous phase $j$ assuming the same density for all gaseous phases:

$$\frac{\partial}{\partial t}(f_i \alpha_j \rho_g) + \nabla(f_i \alpha_j \rho_g \vec{U}_j) = S_{ij} \tag{1}$$

$$\begin{aligned} &\frac{\partial}{\partial t}(\alpha_j \rho_g \vec{U}_j) + \nabla \cdot (\alpha_j \rho_g \vec{U}_j \times \vec{U}_j) = \\ &\nabla \cdot \left[\alpha_j \mu_g (\nabla \vec{U}_j + (\nabla \vec{U}_j)^T)\right] - \alpha_j \nabla p + \alpha_j \rho_g \vec{g} + \vec{M}_j + \vec{S}_{Mj} \end{aligned} \tag{2}$$

with $\vec{M}_j$ being the sum of all interfacial forces acting between the gas phases and the liquid phase from independent physical effects, such as the drag or the lift force. The momentum exchange term $\vec{M}_j$ has to be defined separately for every single gas phase. Inside each velocity group $j$ the continuity equation has to be solved again for each size fraction $i$ including the source term $S_{ij}$, which represents the local transfer of gas phase mass due to bubble breakup and coalescence processes. The corresponding term of $\vec{S}_{Mj}$ in Eq. (2) describes the following transfer of gaseous momentum between different velocity groups. The mechanisms of coalescence and breakup are described using population balance modeling. By including new transfer models, mass is additionally exchanged between the continuous and dispersed gas phases. Thus, transitions between different gas morphologies can be described in general. A fourth polydispersed liquid phase, representing the droplets within this framework, is neglected so far, but constitutes a part of prospective considerations.

The requirement for mesh sensitivity needs to be reconsidered for such a concept. Since the spatial filter width is related to the grid size and all closure models rely on an appropriate choice of this size, the grid size cannot be arbitrarily reduced. The size depends on the concrete interfacial scale, that has to be captured, and the validity of applied closure models.

## 2.2 FREE SURFACE DETECTION

For the continuous gas phase a filtered gas-liquid interface is detected and resolved. In the case of a two-fluid approach the discontinuity at a gas-liquid interface is replaced by a volume fraction gradient. Typically this gradient is characterized by a change of gas volume fraction from 0 to 1 over about three grid cells, as shown in Fig. (2). The detection of an interface is only possible by limited local information, like interfacial area densities or volume fractions. For the new concept a free surface

function is introduced, as shown in Eq. (3). This function detects grid cells, which contain a piece of an interface, by using the volume fraction gradient of the continuous gas. A threshold value of $|\nabla \alpha_{cg}|_{crit}$ is defined as being the gradient that is high enough for an interfacial region to exist.

$$\varphi_{fs} = 0.5 \tanh\left[a_{fs} \Delta x \left(|\nabla \alpha_{cg}| - |\nabla \alpha_{cg}|_{crit}\right)\right] + 0.5 \tag{3}$$

As illustrated in Fig. (2), this method of interface detection results in a loss of information about small waves and instabilities, which are not captured within the computed mesh. Consequently, small wavelength waves and small scale interface deformations are not more identified by their position in space and time and only averaged parameters are known. This loss of information has a reducing influence on mass transfers: some small scale breaking wave may have captured bubbles or some droplets may have formed from a wave crest. Thus, mass transfers will always be underestimated and the loss of information about sub-grid waves has to be modelled by appropriate closure models.

## 2.3 CLUSTER FORCE

An additional interfacial force, working in opposition to the liquid volume fraction gradient, is added to the interfacial momentum transfer equation of the continuous gas phase. It supports the transition from dispersed to continuous gas regions and counteracts the numerical diffusion of the detected interface (Hänsch et al., 2012). If the volume fraction decreases near an interface, the force counteracts the liquid volume fraction gradient and reduces smearing effects.

## 2.4 MODELS FOR THE INTERFACIAL TRANSFERS

Interfacial transfer models for area density and drag of the continuous gas are applied according to the local morphology of the bivalent gas phase. Transitions between dispersed and continuous gas regions have to be taken into account by the models. Closure models are switched depending on the local

volume fraction of the continuous gas. For volume fractions above $\alpha_{cg,crit} = 0.3$ new closure models are applied for the potentially continuous gas, as it is also suggested in the AIAD-model (Höhne and Vallée, 2010). These new models consider the presence of a filtered gas-liquid interface within the multi-field approach. The limit of $\alpha_{cg,crit} = 0.3$ for the dispersed regime is also found by experiments, showing that bubbly flow rarely exceeds this value and normally changes into resolved structures (Toombes and Chanson, 2007). However, the gas can still occur as a dispersed phase, if this critical volume fraction has not been reached, which makes it a bivalent gas phase. The bivalence of the gaseous morphology is necessary in order to enable transitions between dispersed and resolved gas structures, including the possible appearance and evanescence of a particular morphology.

Consequently, three different formulations for the area density and the drag coefficient are applied as demonstrated in Fig. 3. Within the bubble and droplet region the formulations follow the particle model formulation.

$$A_{D,bubb} = 6\alpha_{cg} / d_{cg} \tag{4}$$

$$A_{D,drop} = 6\alpha_{l} / d_{l} \tag{5}$$

However, for first investigations the volume fraction of the liquid was set to a minimum value of $\alpha_l = 1e-07$ inside the continuous gas phase. No droplet phase is considered so far in order to focus on the mass transfers between the two gas phases. $C_{D,bubb}$ for the bubbly regions of the gas phase, where $\alpha_{cg,crit}$ has not been reached yet, follows the correlation of Ishii and Zuber (1979), taking into account different shapes of the bubbles:

$$C_{D,bubb} = \max(C_{D,sphere}, \min(C_{D,ellipse}, C_{D,cap}) \tag{6}$$

including:

$$C_{D,\,sphere} = \frac{24}{\mathrm{Re}}\left(1 + 0.1\mathrm{Re}^{0.75}\right)$$
$$C_{D,\,ellipse} = \frac{2}{3}\sqrt{Eo} \tag{7}$$
$$C_{D,\,cap} = \frac{8}{3}$$

For the droplet phase a constant drag coefficient was applied:

$$C_{D,\,drop} = 0.44 \tag{8}$$

The formulations turned on within the surface layer are shown in Eq. (9) and (10). The interfacial area density depends on both volume fraction gradients of liquid and continuous gas, as such a coupling is necessary for three-field simulations. The drag formulation for the free surface region is changed to the correlation of Höhne and Vallée (2010) accounting for shear stresses $\tau_{w,}$ that occur at the surface, as well as for the slip velocity $u_{slip}$.

$$A_{D,\,fs} = \left(2\left|\nabla\alpha_l\right|\left|\nabla\alpha_{cg}\right|\right) \Big/ \left(\left|\nabla\alpha_l\right| + \left|\nabla\alpha_{cg}\right|\right) \tag{9}$$

$$C_{D,\,fs} = \max\left(0.01\,,\ \frac{2\left[\alpha_l\tau_{w,\,l} + \alpha_{cg}\tau_{w,\,cg}\right]}{\rho_l\ u_{slip}^2}\right) \tag{10}$$

The corresponding blending functions switching the closure between these presented models for the continuous gas phase can be found in Hänsch et al. (2012).

## 2.5 COMPLETE COALESCENCE

A complete gaseous mass transfer replaces all coalescence and breakup processes within continuous gas regions in order to avoid the situation of small bubbles being present inside large gas structures

(Hänsch et al., 2012). Therefore, the entire dispersed gas volume fraction in a grid cell immediately turns into continuous gas, if $\alpha_{cg,crit} = 0.3$ has been reached. This mechanism is turned off within the free surface region, so that mass transfers between different gas phases are possible from and to the filtered interface of the continuous gas. New transfer models describing the breakage and coalescence between such gas morphologies have to be implemented for that purpose in future. The transfer models should be valid for generalized flow situations, which include filtered gas-liquid interfaces, such as the one proposed by Ma et al. (2011).

## 2.6 SUB-GRID WAVE TURBULENCE

Small waves and instabilities, that cannot be resolved as they are smaller than grid size, have been neglected in the simulation so far. The gas-liquid interface is filtered out of averaged information about its residence probability and is represented over about 3 grid cells. However, the sub-grid surface phenomena and disturbances within this surface layer are able to significantly influence the turbulent kinetic energy of the liquid side. Consequently, such small waves are supposed to strongly influence the mass transfer between the gas phases. Since such details cannot be obtained directly, much effort has been spent in their sub-grid modelling. According to Brocchini and Peregrine (2001), the major influence of turbulence on a free surface is caused by the motion of discrete volumes of fluid, called blobs, disturbing the surface. They are given a typical length scale $L$ of dominant surface features resulting from the interaction between turbulence and stabilizing surface effects of gravity $g$ and surface tension $\sigma$. The blobs move with an overall velocity $q$ and a representative kinetic energy density $k_{sw}$. Depending on these two values Brocchini and Peregrine (2001) define different regimes for free surface waves, as shown in Fig. 4. Within the corresponding L, q-diagram the shaded area represents the region of marginal breaking of a surface.

For this substantial range of variation, between a surface that is no longer smooth because of turbulence and a surface that finally breaks up, a lower and an upper bound can be defined analytically. The lower bound, indicating the initial breaking of the surface, can be represented by the creation of new surface caused by the rupture of surface skin. Assuming a linear down welling feature bounded by two convex upward circles, being the smallest possible disturbance giving a surface gradient, the lower bound of the transition region results in:

$$q_l^{\,2} \approx \left(\frac{5}{3}-\frac{\pi}{2}\right)\frac{g_n L}{125}+\frac{(\pi-2)\sigma}{5L} \tag{11}$$

For the upper bound, where the surface has just broken up, a blob is considered to form a spherical drop directly at the surface, which has lost any overall motion. Comparing the turbulent kinetic energy density per unit volume of this blob with the energy of such a surface disturbance per unit surface area, leads to an estimate for the upper bound of:

$$q_u^{\,2} \approx \frac{\pi}{24} g_n L+\frac{\pi\sigma}{2L} \tag{12}$$

Thus, the turbulent kinetic energy created by blobs of different length scales can be estimated by:

$$k_{sw} = 0.5\left(q_u^{\,2} - q_l^{\,2}\right) \tag{13}$$

However, as it is pointed out by Coste (2013), the model of Brocchini and Peregrine considers only horizontal flows, where gravity indeed has stabilizing effects on small waves occurring at a free surface. But when considering the model in a more general framework, where gas-liquid interfaces also appear inclined or even vertical, gravity does not necessarily stabilize the interface. In cases where liquid is located above the gas phase, gravity can even have an inverse effect and destabilize the interface. In order to account for such situations Eq. (12) and (13) include $g_n$:

$$g_n = \vec{g} \cdot \vec{n} \tag{14}$$

being the dot product of gravity and the interface normal vector, which is defined by using the volume fraction gradient of the liquid phase:

$$\vec{n} = \frac{\Delta\alpha_l}{|\Delta\alpha_l|} \tag{15}$$

Thus, the expression for $g_n$ turns 0 in cases where the interface appears vertical, and it even turns negative when liquid is overlapping gas regions.

In the simulations the turbulence of the liquid phase is described by the k-ω based SST-model. For the inclusion of sub-grid wave turbulence a corresponding source term is added to the turbulence production term in the transport equation of turbulent kinetic energy k of the liquid phase. It is blended in within the free surface region detected by the function in Eq. (3).

$$P_{kswt} = \varphi_{fs} \frac{2}{3} \frac{\partial U_{li}}{\partial x_i} \rho_l k_{sw} \tag{16}$$

The sub-grid source term depends on both the liquid velocity gradient and the density. The length scale $L$ is set to the chosen grid size $\Delta x$, since all surface features smaller than or equal to this size have to be modelled. The way the model of Brocchini and Peregrine (2001) was interpreted and included into the turbulent transport equation of $k$ has also been tested and validated by Höhne (2013).

## 3 DAM-BREAK SIMULATION WITH AN OBSTACLE

The introduced concept can be applied to any two-phase flow situation, that includes small- and large scale gas structures. This paper presents only one demonstration case, which is a dam-break with an obstacle. The same test case of a liquid column collapsing and hitting an obstacle (Koshizuka et al.,

1995) has also been used by other authors for testing their interface tracking or interface capturing methods (e. g. Ubbink, 1997; Muzaferija, 1999; Greaves, 2006). By using the new concept the case is intended to demonstrate the transfer from a continuous gas phase into dispersed structures being entrained by the breaking wave. Later these dispersed structures are supposed to rise back to the surface and re-coalesce with the continuous gas above, leading to a final separation of the phases. In the experiment a box made of glass with an obstacle on the bottom wall is recorded by a video camera. The water column inside is supported by a vertical wall, which is drawn up rapidly (~ 0.05s) for the beginning of the process.

The simulations are performed with the CFX-code 14.0. The computational domain is changed to a square tank to avoid a spill over of water droplets. Therefore, the original height is increased to 0.584m compared to the experimental setup, which is an open topped container as indicated by the dotted line in Fig. 5. The quasi two-dimensional grid contains 146x146 elements. With an equidistant grid of $\Delta x$=4mm the modeled sub-grid waves according to the L, q-Diagram in Fig. 3 are supposed to be knobbly wave structures. The simulations are performed using a three-field two-fluid setup. Two gas phases are defined consisting of 5 bubble size classes as shown in Table 1. The fluid properties are set to the physical values of water and air at 25°C. The interfacial transfer models applied for the different fluid pairs are summarized in Table 1. Mass transfer processes among the bubble size classes are described by using the model of Prince and Blanch (1990) for coalescence and the model of Luo and Svendsen (1996) for breakup. The liquid column was initialized in the lower left corner with a turbulence intensity of 10% and an eddy viscosity ratio of 100. These parameters are meant to represent the fact of initial distortion of the column by removal of the internal wall in the experiment. The column is applied with an initially smeared free surface region in order to improve convergence during the first time steps. At the walls no slip condition is applied for the liquid phase, and free slip condition

for both gas phases. An opening boundary condition closes the domain at the top with a relative pressure of 0Pa. At the front and back planes symmetry condition is used. The local pressure of a point at half the height of the obstacle, as shown in Fig. 5, is monitored during the simulation.

The high resolution scheme is applied for the advection terms to minimize the effect of numerical diffusion. For transient time integration the fully implicit second order backward Euler scheme is used with a constant time step of 0.5ms. For each time step convergence has to be achieved within 5 to 30 inner coefficient loops using the averaged residual convergence criteria of RMS=1e-04.

The simulations are performed with both a constant drag coefficient $CD_{fs}$=0.01 within the free surface region and the drag formulation in Eq. (10). Furthermore, results are compared for different breakup efficiencies of $F_B$=1.0 and 10, as well as with the implementation of the new source term for sub-grid wave turbulence in Eq. (16).

# 4 RESULTS

The general flow behaviour in the first half of a second is demonstrated and compared to experimental photos in Fig. 6. Initial conditions differ from the experiment as no gas movements occur in the simulation, while in the experiment the free surface is already disturbed by removal of the internal wall. The detected free surface is represented in an enclosed manner as can be seen from the computational results.

After 0.1s the leading edge of the collapsing water column has not reached the obstacle yet. However, in the experiment a thin liquid layer, rushing over the bottom of the tank, has already been blocked by the obstacle.

After 0.2s the movement of the leading edge has been distracted by the obstacle in both simulation and experiment. This rise of pressure can be observed in the computed pressure line of the monitor point

shown in Fig. 7. Unfortunately no experimental pressure data are available. A water tongue bounces up in the direction of the opposite wall. In the experiment a strong formation of droplets occurs from the upper part of the water tongue, which cannot be reproduced by the simulation so far. The capture of these droplets requires a four-field simulation, which additionally takes into account a polydispersed droplet phase. The water tongue further induces a large eddy in the center of the domain, as can be seen from the velocity vectors of the continuous gas phase.

The tongue continues its movement towards the wall after 0.3s. There is a good agreement in shape of the interface despite the use of an averaged Euler-Euler approach within a relatively coarse mesh, when compared to previous studies using compressive differencing schemes (Ubbink, 1997). The central eddy enhances the prolongation of the water tongue towards the upper right corner of the domain.

At 0.4s the tongue has impinged on the wall closing an area of air beneath it and entrapping a small gas structure close to the wall. The water sheet begins to fall due to gravity, but the trapped air on the bottom provides resistance against this downward motion (Ubbink, 1997). The computed vectors of superficial gas velocity within this region indicate the formation of a second eddy. The generation of a secondary water tongue starts at the obstacle due to pressure repulsion when the water tongue impinges on the wall. A corresponding second peak of pressure value appears for 0.34s in Fig. 7.

At 0.5s the sheet of water continues its downward movement at the wall and the trapped air will eventually burst through the water enhanced by the eddy in the lower part. The secondary water tongue is reaching over the obstacle and moves into the trapped air region beneath the first water sheet. The small gas structure at the wall disappears at this point.

After 0.6s a very thin sheet of water is left and the secondary tongue has impinged against the bottom wall, trapping a smaller space of air next to the obstacle. A third small pressure peak is also indicated at 0.54s in Fig. 7. The water sheet on the right wall contains a bubble, which has formed due to the

downward motion of the interface. It is hard to identify this structure in the experimental photo due to low quality, but it was also reproduced by Ubbink (1997) in former calculations.

In general the comparison proves that the new model is able to capture the main characteristics of the separated flow. The shape of horizontal and vertical interfaces corresponds well with the images and former interface capturing simulations. Furthermore, the timescale of simulation and experiment agrees. However, in the experiment some water spills over and leaves the tank, so that no mass conservation can be guaranteed. When comparing simulation and experiment this fact has to be regarded.

The benefits of the new concept lie within the description of the subsequent part of the process. First, the modeling of bubble capture by breaking waves is now treated as an actual mass transfer between a continuous and a dispersed gas phase. Therefore, appropriate physical breakup models can be applied. Second, once the dispersed gas has been entrained, it can be described using the MUSIG model taking into coalescence and breakup processes. As discussed in Hänsch et al. (2013), Volume-of-Fluid methods usually end up in diffusive volume fraction captured underneath the surface as a numerical artifact. Furthermore, included interface capturing schemes are physically not valid for multi-scale simulations, as they lead to an artificial aggregation of small with large scale gas structures. On the contrary, the new concept describes a physical transfer to a polydispersed gas instead. After the enclosure of a large amount of gas and the generation of turbulent kinetic energy, the breakup from the free surface region to the dispersed gas phase starts in the lower right corner of the domain. The mass transfer to the dispersed gas phase occurs wherever the turbulent kinetic energy reaches high values within the detected free surface region.

The entrainment of dispersed gas starts after 0.7s and reaches its peak at 1.1s, as shown in Fig. 8. The use of the new drag formulation hardly influences the results. The motion of the gas-liquid interface

does not change and also the amount of entrained dispersed gas is not affected. The shear stresses within the free surface region are too small to make the drag coefficient exceed the defined minimum value of 0.01. Obviously, the correlation changes the coefficient in cases where higher velocities occur within the free surface region. All further simulations were performed using the new drag correlation of Eq. (10). As it is shown in Fig. 9 for 1.0s, large continuous gas structures are left underneath the free surface. Although structures of this size cannot be fairly recognized in the experimental image, no continuous structures seem to be left in the experiment. Considering the good agreement of continuous gas structures in the first part of the process, as demonstrated in Fig. 6, this indicates an underestimation for the mass transfer from the free surface region to the dispersed gas. Two different parameters were changed to investigate their influence on this mass transfer: the breakup efficiency $F_B$ on the one hand, and the turbulence level within the free surface region on the other hand, using the new source term for sub-grid wave turbulence.

The dispersed gas holdup for the different cases is compared in Fig. 8. The increase of breakup efficiency to $F_B$=10 leads to a peak value of dispersed gas holdup, which is three times larger than the result using the default value of $F_B$=1. The peak occurs at the same time at 1.1s. The trapped bubble at the wall at 0.6s and all continuous structures underneath the free surface in Fig. 9 appear smaller for that case due to the increased mass transfer to the dispersed gas phase. The bubble size distribution is shifted towards smaller bubble sizes within the entire computational domain. The whole entrainment process is decelerated, when compared to the result with default breakup efficiency in Fig. 8. The re-coalescence of dispersed bubbles with the surface is still not finished after 3.0s. Since a change of the breakup efficiency to $F_B$=10 leads to a bubble size distribution shifted towards smaller sizes within the whole domain, these smaller bubbles rise slower and decelerate the entire entrainment process.

By using the source term for sub-grid wave turbulence, the formation of dispersed gas starts much earlier at 0.2s with the peak gas holdup at 0.9s. Fig. 8 shows that the maximum amount of entrained dispersed gas at 0.9s is about two times larger than without considering the sub-grid waves. In contrast to the previous results, where the amount of entrained gas increases until 1.1s, the process calms down earlier after applying the sub-grid wave turbulence term, which fits better to the experimental image for 1.0s. The whole entrainment process is finished at 2.2s like for the default case. This demonstrates that the source term is only activated temporarily and locally at the free surface. Thereby it only enhances the mass transfer to the dispersed gas within the free surface region, without affecting the coalescence and breakup processes underneath the water level as shown in Fig. 9. A higher amount of turbulent kinetic energy is produced in the first seconds of the simulation at the water tongue moving towards the wall, as demonstrated in Fig. 10. The dispersed gas initially appears at the tip of the water tongue. This is difficult to confirm by the experimental images, but seems reasonable due to an expected high level of interfacial distortion at this moment and location. The main air entrainment occurs after the water tongue has impinged at the wall at 0.5s. At this point in time the sub-grid source term is mainly activated in the outer region of the impingement area, as illustrated in Fig. 11. This is a region where interface capturing methods predict highly disturbed, knobbly surfaces, making the activation of the source term at this location reasonable (Hänsch et al., 2013).

The computed water height at the left wall for the whole process is compared to the experimental height in Fig. 12. Therefore, the experimental photos were analyzed using a similar algorithm to the one presented by Montoya et al. (2012). In this algorithm, the image is subjected to a pre-treatment with a series of filters, then segmented into the determined regions of interest, and finally binarized and analyzed. The results for the water level are extracted, as demonstrated for a few points at 1.0s in Fig. 13. The comparison of water level height at the left wall in Fig. 12 shows agreement to the obtained

experimental data for all the cases until 0.5s. As can be seen from Fig. 9 and 12, it is obvious that the addition of sub-grid wave turbulence has a strong influence on the motion of the free surface. The main difference can be identified for the splashing phenomena at the left wall for 1.0s, as demonstrated in Fig. 12. Without considering the sub-grid wave turbulence term, the back-splashing of water was underestimated. After including the source term the water height at the left wall agrees better with the experimental data. This improvement is strongly related to the advanced description of air entrainment under the surface. The new sub-grid wave term enhances the mass transfer to the dispersed gas and thus increases the water level within the whole computational domain. However, the experimental data are represented by low quality images with inadequate light conditions, making the automatic binarization of the image processing algorithm less reliable for the validation of that data. Moreover, experimental data for the relevant part after 1.0s are not available anymore. It is suggested to rerun the experiment to provide both high quality pictures and quantitative data for a validation of new models. In future the new sub-grid source term for small waves should be combined with an appropriate entrainment model like the one proposed by Ma et al. (2011), in which the liquid turbulent kinetic energy directly influences the mass transfer to the dispersed gas. This model is supposed to predict the location and rate of air entrainment for generic free surface flows and fits the needs of a generalized two-phase flow approach.

# 5 CONCLUSION

The recently developed GENTOP-concept describes transitions between polydispersed and continuous gas phases. It introduces new generalized formulations for the interfacial transfers by filtering large interfaces within the MUSIG-framework. The concept was improved by introducing an appropriate drag-formulation, which takes into account the shear stresses occurring within the free surface region.

Furthermore, a model for sub-grid wave turbulence was included, which is added as a source term for liquid turbulent kinetic energy. The source term increases the turbulent kinetic energy of the liquid phase due to surface features, which are normally filtered out using an URANS-approach. The extended GENTOP-concept was applied to the test case of a collapsing liquid column hitting an obstacle. All simulations could capture the main flow characteristics of the dam-break case by accurately reproducing the motion of the gas-liquid interface. The results agree well with the experimental photos, as well as with computational results obtained by various authors. The height of the water level at the left wall fits to image processing data obtained from the photos. The change of the free surface drag coefficient to the new correlation hardly changed the computational results, so that all further simulations were performed applying it. The main benefits of the new concept are twofold and lie within the description of the subsequent part of the experiment, when gas is entrained under the surface and turns into a dispersed phase. First, the bubble capture by breaking waves can now be treated as an actual mass transfer to a dispersed gas phase using physical breakup models. Second, once the gas has been entrained it is described by the MUSIG-model using appropriate closure models. The gas forms a bubble size distribution which evolves from the surrounding flow field conditions. The entrained bubbles then rise to the surface and transfer back into the continuous gas phase, leading to the final flow field separation. In general, the model predicts many continuous gas structures underneath the surface, indicating that an advanced air entrainment model is needed. By adding the new source term for sub-grid wave turbulence the entrainment process is accelerated and the back-splashing water level at the left wall fits better to the experimental data. A main part of the ongoing work is the implementation of an appropriate entrainment model, that harmonizes with the improved description of turbulence within the free surface layer. Furthermore, the experiments should be rerun to provide both

high quality pictures and quantitative data for a validation of new models, in particular for the last part of the process acquiring high quality images.

This work is carried out in the frame of a current research project funded by the German Federal Ministry of Economics and Technology, project number 150 1411.


## 6 REFERENCES

Bestion, D., 2012. The difficult challenge of a two-phase CFD modeling of all flow regimes, Proc. CFD4NRS-4, Daejeon, South Korea, September 10-12.

Brocchini, M. and Peregrine, D.H., 2001. The dynamics of strong turbulence at free surfaces. Part 1. Description, J. Fluid Mech., Vol. 449, 225–254.

Černe, G.; Petelin, S.; Tiselj, I., 2001. Coupling of the Interface Tracking and the Two-Fluid Models for the Simulation of Incompressible Two-Phase Flow. J. Comput. Phys. 171, 776-804.

Coste, P., 2013. A large interface model for two-phase CFD. Nucl. Eng. Des. 255, 38-50.

Greaves, D.M., 2006. Simulation of viscous water column collapse using adapting hierarchical grids, Int. J. Numer. Meth. Fluids, Vol. 50, 693–711.

Hänsch, S.; Lucas, D.; Krepper, E.; Höhne, T., 2012. A multi-field two-fluid concept for transitions between different scales of interfacial structures, Int. J. Multiphase Flow, Vol. 47, 171–182.

Hänsch, S., 2013. Comparative simulations of free surface flows using VOF-methods and a new approach for multi-scale interfacial structures. Proc. ASME FEDSM, Incline Village, Nevada, USA, July 7-11.

Höhne, T. and Vallée, C., 2010. Experiments and numerical simulations of horizontal two phase flow regimes using an interfacial area density model, JCMF, Vol. 2, 131–143.

Höhne, T., 2013. Modelling and validation of turbulence parameters at the interface of horizontal multiphase flows. Proc. 8th ICMF, Jeju, South Korea, May 26-31.

Ishii, M. and Zuber, N., 1979. Drag coefficient and relative velocity in bubbly, droplet or particulate flows. AIChE J. 25 (5), 843-855.

Koshizuka, S.; Tamako, H.; Oka, Y., 1995. A particle method for incompressible viscous flow with fluid fragmentation, Comp. Fluid Dyn. J., Vol. 4, pp. 29–46.

Krepper, E.; Lucas, D.; Frank, T.; Prasser, H.-M. & Zwart, P., 2008. The inhomogeneous MUSIG model for the simulation of polydispersed flows. Nucl. Eng. Des. 238, 1690–1702.

Luo, H. and Svendsen, H. F., 1996. Theoretical model for drop and bubble break-up in turbulent flows. AIChE J. 42 (5), 1225-1233.

Ma, J.; Oberai, A.A.; Drew, D.A.; Lahey Jr, R.T.; Hyman, M.C., 2011. A Comprehensive Sub-Grid Air Entrainment Model for RaNS Modeling of Free Surface Bubbly Flows, JCMF, Vol. 3, 41–56.

Montoya Z., G.A.; Deendarlianto; Lucas, D.; Höhne, T.; Vallée, C., 2012. Image-Processing-Based Study of the Interfacial Behavior of the Countercurrent Gas-Liquid Two-Phase Flow in a Hot Leg of a PWR, Science and Technology of Nuclear Installations.

Muzaferija, S. and Perić, M., 1999. Computation of free surface flows using interface-tracking and interface-capturing methods. In O. Mahrenholtz, M. Markiewicz (eds.), Nonlinear Water Wave Interaction, Chap. 2, 59-100, WIT Press, Southampton.

Prince, M. J. and Blanch, H. W., 1990. Bubble coalescence and break-up in air-sparged bubble columns. AIChE J. 36 (10), 1485-1499.

Štrubelj, L.; Tiselj, I.; Mavko, B., 2009. Simulations of free surface flows with implementation of surface tension and interface sharpening in the two-fluid model. Int. J. Heat Fluid Flow 30, 741-750.

Tomiyama, A. and Shimada, N., 2001. (N+2)-Field Modeling for Bubbly Flow Simulation. Comp. Fluid Dyn. J., Vol. 9 (4), 418-426.

Tomiyama, A.; Sakoda, K.; Hayashi, K.; Sou, A.; Shimada, N.; Hosokawa, S., 2006. Modeling and Hybrid Simulation of Bubbly Flow. Multiphase Sci. Tech., 18(1), 73-110.

Toombes, L. and Chanson, H., 2007. Surface waves and roughness in self-aerated supercritical flow, Environ Fluid Mech, Vol. 7, 259–270.

Ubbink, O., 1997. Numerical predictions of two fluid systems with sharp interfaces, *Ph.D thesis*, University of London / Imperial College.

Yan, K. and Che, D., 2010. A coupled model for simulation of the gas–liquid two-phase flow with complex flow patterns. Int. J. Multiphase Flow 36, 333–348.

FIGURES

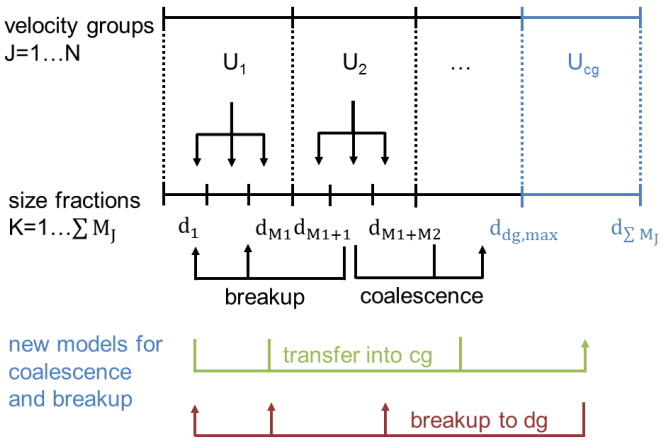


Fig. 1 Extension of the inhomogeneous MUSIG-Model (Hänsch et al., 2012).

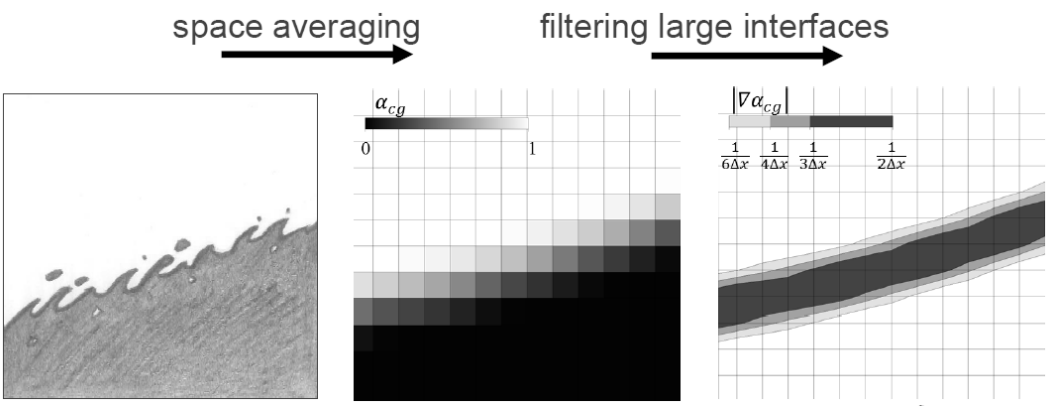


Fig. 2 Scheme for the free surface detection in GENTOP.

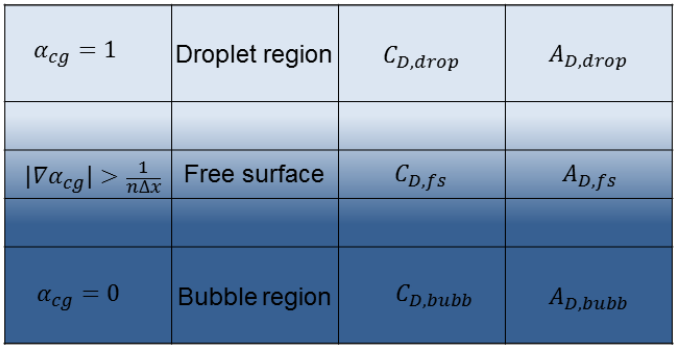


Fig. 3 Bivalence of the continuous gas phase (Hänsch et al., 2012).

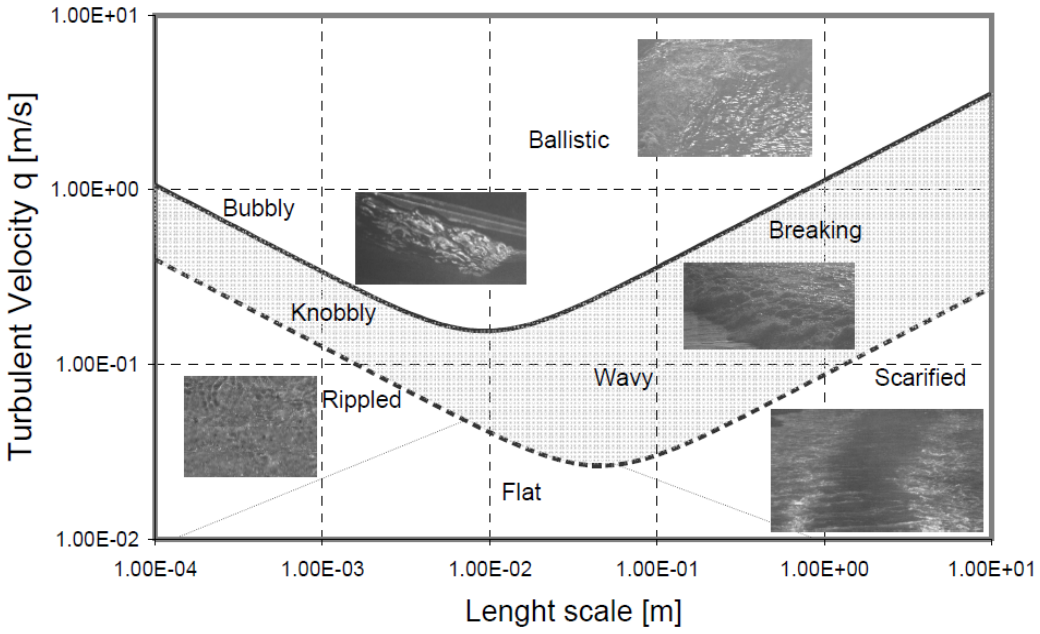


Fig. 4 L, q-diagram of surface waves (Brocchini and Peregrine, 2001).

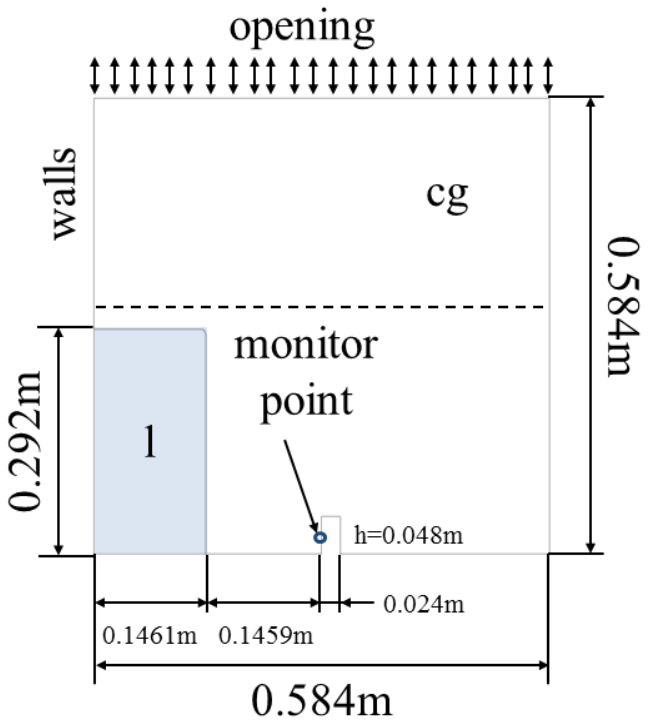


Fig. 5 Computational domain and boundary conditions.

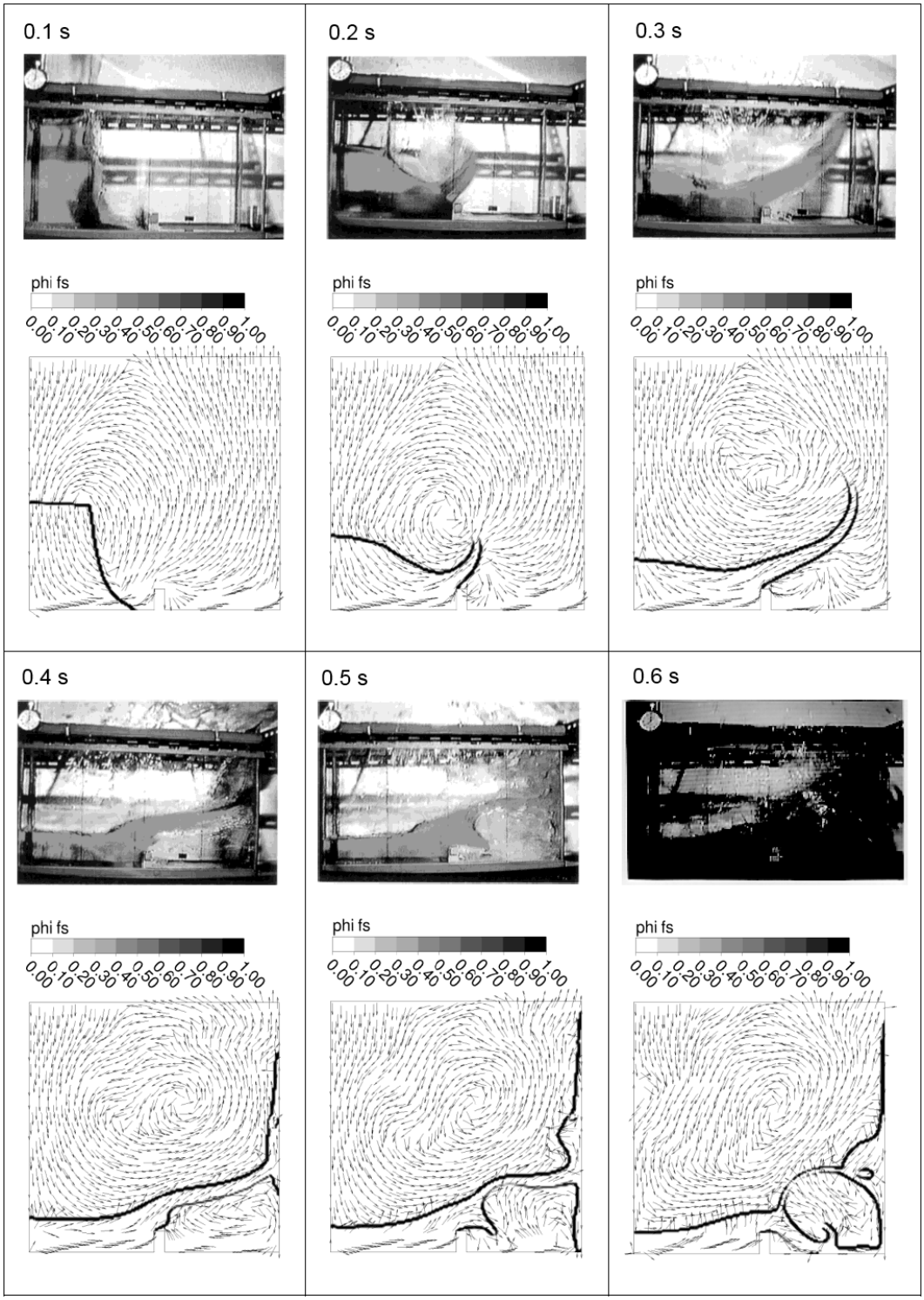


Fig. 6 Free surface detection function and superficial gas velocity vectors compared to the experimental photos (Koshizuka et al., 1995; Ubbink, 1997).

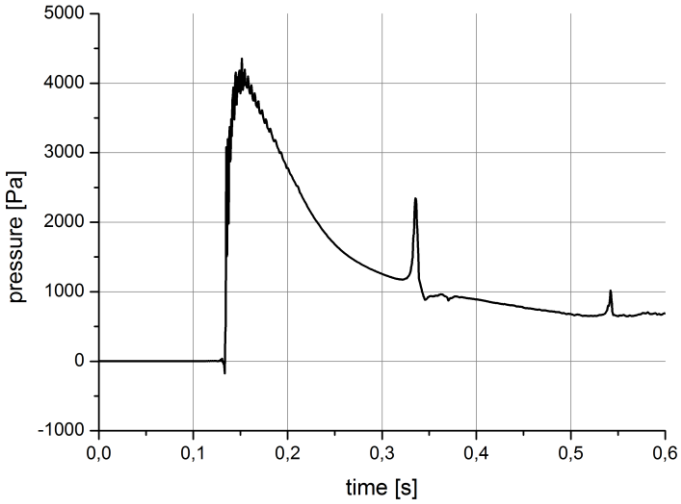


Fig. 7 Pressure at the monitor point over time.

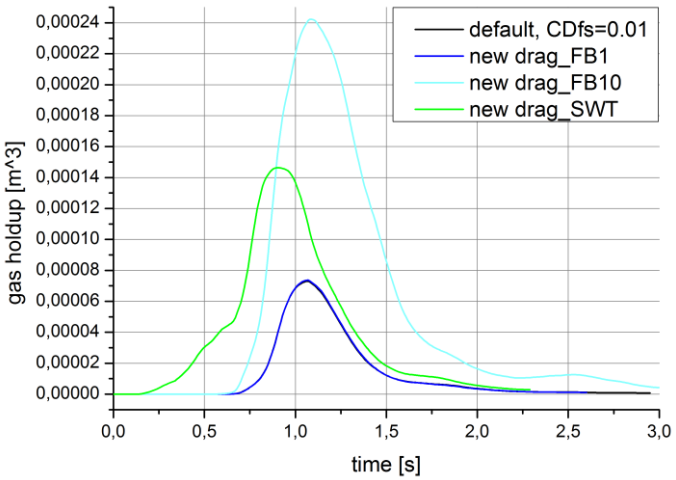


Fig. 8 Gas holdup for the dispersed gas phase with default values, new drag formulation, increased breakup efficiency and sub-grid wave turbulence.

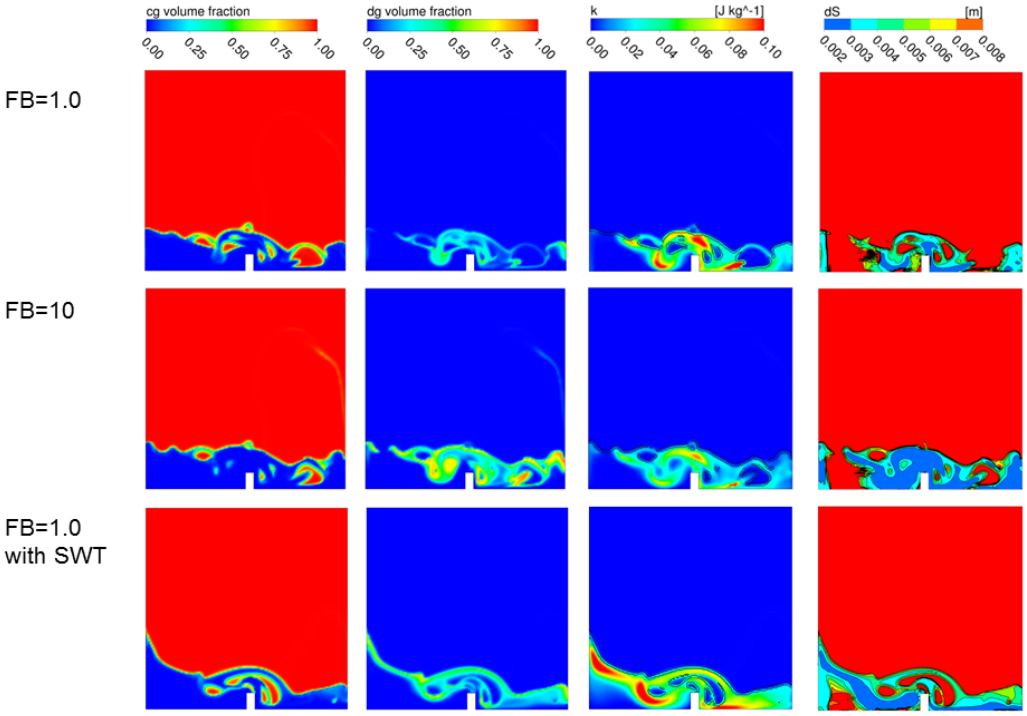


Fig. 9 Computational results for $F_B$=1.0, $F_B$=10 and SWT after 1.0s, from left to right: gas volume fraction field of cg and dg, liquid turbulent kinetic energy k and isolines of $\varphi_{fs}$=0.5 enclosing the main part of the free surface region, bubble size distribution represented by Sauter mean diameter $d_S$.

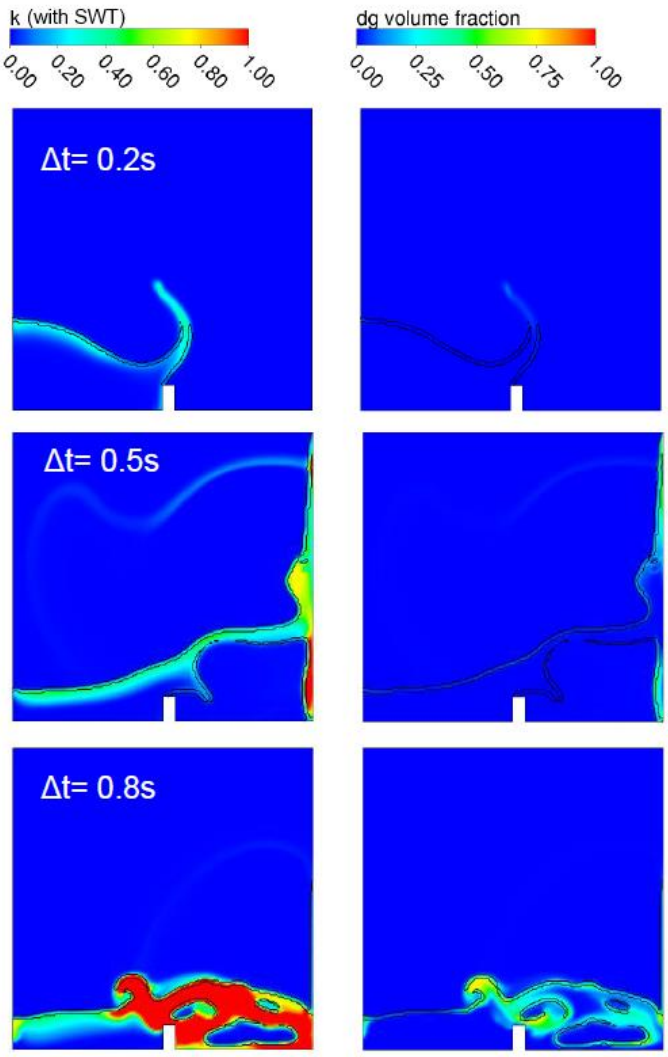


Fig. 10 Turbulent kinetic energy k of the liquid phase with new sub-grid wave source term and dg volume fraction field, isolines of $\varphi_{fs}$ =0.5 enclosing the free surface region.

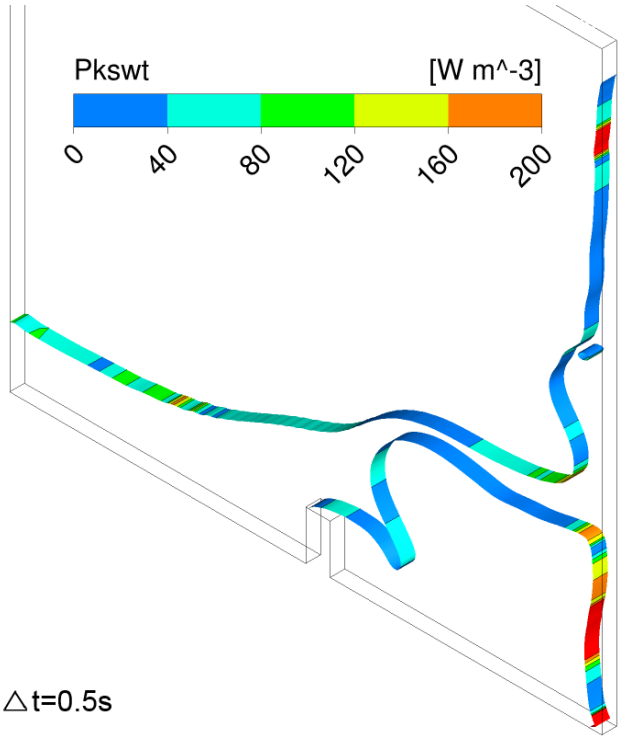


Fig. 11 Source term for sub-grid wave turbulence on the isosurfaces of $\alpha_{cg}$=0.5.

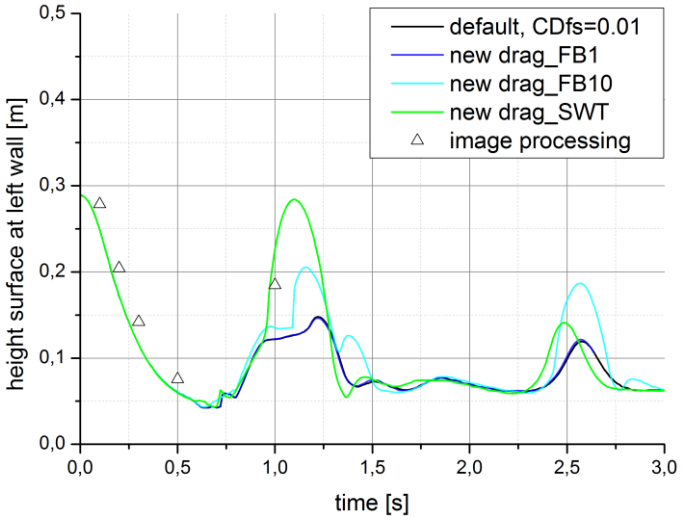


Fig. 12 Free surface height at the left wall of the domain compared to the experimental data.

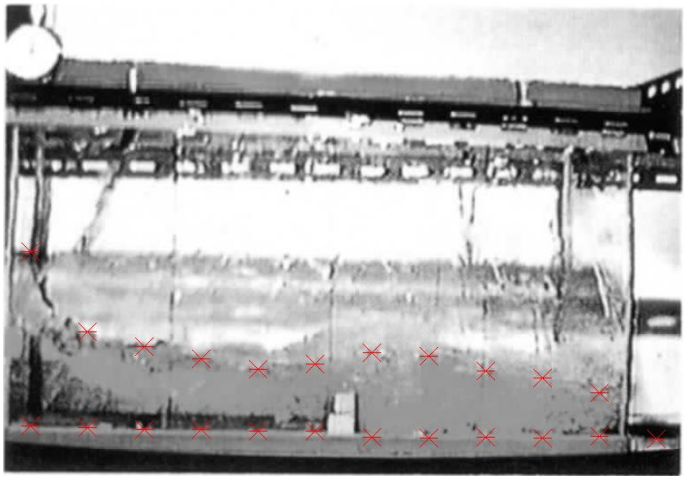

Fig. 13 Back-splashing at 1.0s with data points after image processing.

TABLES

Table 1 Applied models for interfacial transfers.

| $U_g$ | $d_g$ | | | | $c_g$ |
|---|---|---|---|---|---|
| Morphology | polydispersed | | | | continuous |
| Bubble classes | 1 | 2 | 3 | 4 | 5 |
| $d_i$ [mm] | 2 | 4 | 6 | 8 | ≥10 |
| Interphase transport | Particle Model | | | | $A_{D,cg}$ |
| Drag | Ishii Zuber | | | | $C_{D,cg}$ |
| Turbulence | Dispersed Phase Zero Equation | | | | |
| Lift force | Tomiyama | | | | None |
| Turbulent Dispersion | Favre Averaged | | | | None |
| Cluster force | None | | | | Hänsch |